Acta Crystallographica Section D
Biological Crystallography
ISSN 0907-4449

Structural basis for the high-affinity binding of pyrrolotriazine inhibitors of p38 MAP kinase

John S. Sack,[a]* Kevin F. Kish,[a] Matthew Pokross,[a] Dianlin Xie,[b] Gerald J. Duke,[b] Jeffrey A. Tredup,[b] Susan E. Kiefer[b] and John A. Newitt[b]

[a]Department of Macromolecular Crystallography, Bristol-Myers Squibb Research and Development, PO Box 4000, Princeton, NJ 08543-4000, USA, and [b]Department of Gene Expression and Protein Biochemistry, Bristol-Myers Squibb Research and Development, PO Box 4000, Princeton, NJ 08543-4000, USA

Correspondence e-mail: john.sack@bms.com

Received 25 February 2008
Accepted 11 April 2008

PDB References: p38 MAP kinase–inhibitor complexes, 2rg6, r2rg6sf; 3bv3, r3bv3sf.

The crystal structure of unphosphorylated p38α MAP kinase complexed with a representative pyrrolotriazine-based inhibitor led to the elucidation of the high-affinity binding mode of this class of compounds at the ATP-binding site. The ligand binds in an extended conformation, with one end interacting with the adenine-pocket hinge region, including a hydrogen bond from the carboxyl O atom of Met109. The other end of the ligand interacts with the hydrophobic pocket of the binding site and with the backbone N atom of Asp168 in the DFG activation loop. Addition of an extended benzylmorpholine group forces the DFG loop to flip out of position and allows the ligand to make additional interactions with the protein.

1. Introduction

The p38 mitogen-activated protein (p38 MAP) kinase has been shown to play a key role in the regulation of the cellular response to external stress signals. The p38-dependent pathway mediates the production of proinflammatory cytokines such as interleukin-1β (IL-1β) and tumor necrosis factor α (TNF-α); inhibitors of p38 MAP kinase thus have the potential to aid in the treatment of rheumatoid arthritis and other inflammatory diseases (see Saklatvala, 2004).

The design of small-molecule inhibitors of p38 MAP kinase has been the subject of major efforts by pharmaceutical companies and a wide variety of different inhibitors have been reported. The development of many of these compounds has been aided by the use of X-ray crystallography to show the precise mode of ligand binding; some examples include substituted pyridinyl imidazoles (Tong *et al.*, 1997), dihydroquinazolinones (Stelmach *et al.*, 2003) and 4-azaindoles (Trejo *et al.*, 2003). The crystal structures of these compounds in complex with p38 MAP kinase have shown that most inhibitors bind in the same site and mimic many of the same interactions as ATP. However, in an effort to increase the specificity of these ligands for p38 MAP kinase over other ATP-binding kinases, additional interactions between the protein and the inhibitor are usually present (Adams *et al.*, 2001). For example, many inhibitors utilize interactions with the gatekeeper residue Thr106 in order in increase their specificity for p38 MAP kinase (Lisnock *et al.*, 1998; Kumar *et al.*, 2003).

Most of the small-molecule inhibitors for which structures have been determined have been shown to bind to p38 MAP kinase without affecting the overall structure of the ATP-binding site. However, one series of diarylurea compounds have been reported to bind in a site adjacent to the normal ATP-binding site and to force the residues Asp-Phe-Gly (DFG) at the start of the activation loop in p38 to flip out of

position by about 10 Å. This major conformational change in the protein creates a new hydrophobic pocket in the binding site which can be utilized for additional interactions. This phenomenon has been referred to as the DFG-out conformation (Pargellis *et al.*, 2002; Regan *et al.*, 2002). This motion of the DFG loop has also been reported for anilinoquinazoline-based inhibitors (Cumming *et al.*, 2004).

In an effort to aid in the development of a series of pyrrolotriazine-based inhibitors of p38 MAP kinase, we have determined the single-crystal structures of two representative compounds from this class of inhibitor bound to p38 MAP kinase. The two ligands, which both have high-affinity binding to p38 MAP kinase (Table 1), differ in the replacement of a methoxyamide by an extended benzylmorpholine group (Fig. 1). Comparison of these two structures, as well as comparison with other reported structures of p38 complexes, has enhanced our understanding of the mode of binding of these compounds.

2. Experimental procedures

The pyrrolotriazine inhibitors of p38 were provided by Shuqun Lin from the Department of Discovery Chemistry, Bristol-Myers Squibb Research and Development. Details of the syntheses and subnanomolar potencies are described elsewhere (Wrobleski *et al.*, 2008; Hynes *et al.*, 2008). Protein

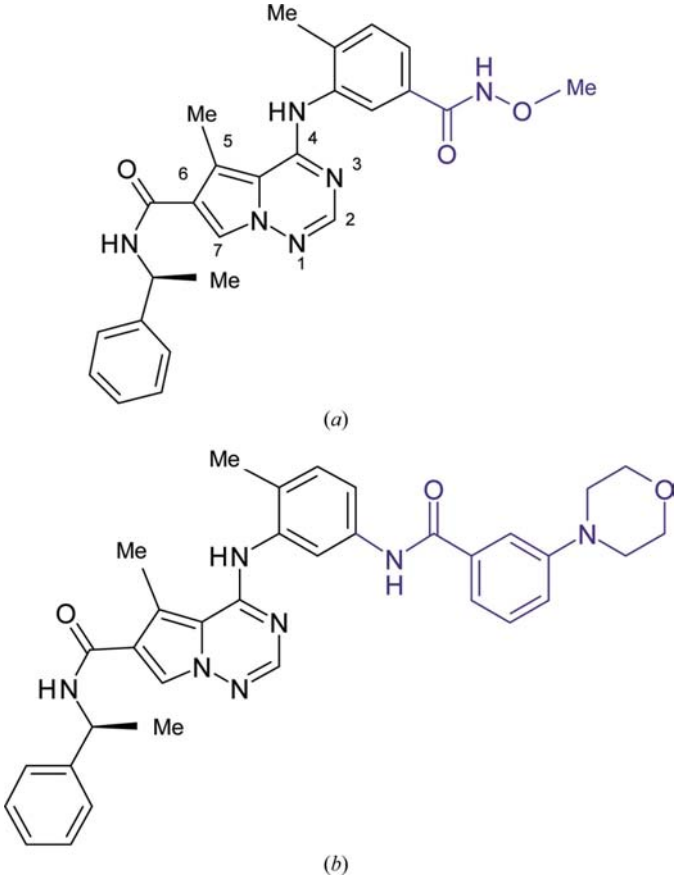

Figure 1
Structure of (*a*) inhibitor 1 and (*b*) inhibitor 2.

Table 1
IC_{50} values for p38α MAP kinase.

Compound	IC_{50} (n*M*)
Inhibitor 1†	2.2
Inhibitor 2‡	0.4
BIRB-796§	8.0

† Hynes *et al.* (2008). ‡ Wrobleski *et al.* (2008). § Pargellis *et al.* (2002).

concentrations were determined by the Bradford protein assay (Bio-Rad) using a bovine serum albumin standard curve.

The *Escherichia coli* expression vector for recombinant His-tagged human p38α was constructed by PCR amplification of the coding region from a different expression vector containing the p38 cDNA (NCBI RefSeq NM_139012) with primers encoding an N-terminal His_5 tag and flanking *Nco*I and *Bam*HI sites. The product was inserted into pET28a (Novagen) between the *Nco*I and *Bam*HI sites to yield the final N-His5-p38α-pET28a vector that encoded MAHHHHH– fused directly to p38α amino-acid residues 2–360 (corresponding to NCBI RefSeq NP_620581) under control of the T7 *lac* promoter.

2.1. Preparation of inhibitor 1 complex for X-ray crystallography

The p38 protein used in the cocrystallization with inhibitor 1 was expressed in *E. coli* by transforming the BL21 (DE3) strain with the N-His5-p38α-pET28a plasmid and spreading on LB plates containing 30 µg ml^{-1} kanamycin sulfate. A single transformant colony was picked, inoculated into 50 ml defined M9-glucose medium with casamino acids (Difco) and trace minerals (see supplementary material for medium recipe[1]) plus 30 µg ml^{-1} kanamycin sulfate and grown to saturation at 310 K overnight. The cells were pelleted, resuspended in 2 ml fresh medium and added in a ratio of 1:1000 to inoculate 1 l shake-flask cultures (in 2 l flasks) of M9-glucose/casamino acids medium with 30 µg ml^{-1} kanamycin sulfate. The cultures were grown at 310 K in a shaking incubator (225 rev min^{-1}) until they reached an optical density at 600 nm of 0.8. The cultures were chilled on ice for 30 min and 0.5 m*M* isopropyl β-D-1-thiogalactopyranoside (IPTG) was added. The induced cultures were incubated at 293 K for 18 h in a shaking incubator (225 rev min^{-1}) before harvesting (by centrifugation) and freezing the cell paste. The His_5-p38α protein was purified at 277 K by suspending 20 g frozen cell paste in 200 ml buffer *A* [20 m*M* Tris–HCl pH 8.0, 50 m*M* NaCl, 5%(*v*/*v*) glycerol] plus 1 m*M* EDTA, 1 m*M* TCEP, one Complete EDTA-free protease-inhibitor tablet (Roche) per 50 ml, 10 m*M* DTT and passing once through a homogenizer (Niro-Soavi Panda) at 85 MPa. The lysate was clarified by sedimentation (Beckman Ti45 rotor; 40 000 rev min^{-1} for 1 h) and the supernatant was loaded onto a Q-Sepharose Fast Flow (GE Healthcare) column (2.6 × 11 cm) equilibrated with buffer *A* plus 2 m*M* DTT. The p38 protein was eluted with a

[1] Supplementary material has been deposited in the IUCr electronic archive (Reference: EN5295). Services for accessing this material are described at the back of the journal.

linear gradient of NaCl in buffer *A* plus 2 m*M* DTT. Gradient fractions at approximately 250–400 m*M* NaCl containing p38 (identified by SDS–PAGE analysis) were pooled and loaded onto a 5 ml HisTrap HP column (GE Healthcare) equilibrated with buffer *B* [20 m*M* Tris–HCl, 10 m*M* imidazole, 5%(*v*/*v*) glycerol, 300 m*M* NaCl, 2 m*M* DTT pH 7.5]. The column was washed with 15 m*M* imidazole in buffer *B* and the p38 protein was eluted with approximately 125 m*M* imidazole in a linear gradient to 250 m*M* imidazole in buffer *B*. The pooled fractions (13.5 ml) were concentrated to 4 ml and loaded onto a Superdex 200 column (1.6 × 60 cm) equilibrated with buffer *C* [25 m*M* Tris–HCl pH 7.5, 50 m*M* NaCl, 5%(*v*/*v*) glycerol, 0.5 m*M* EDTA, 2 m*M* DTT]. The purified p38 protein was pooled from the center of the major peak at an elution volume consistent with monomeric p38. The final purity was greater than 95% by SDS–PAGE analysis and the recovery was 40 mg purified His_5-p38α per litre of culture. The observed mass of the final product was 41 912 by electrospray ionization mass spectrometry, which is consistent with the predicted mass of expressed protein after the expected co-translational removal of the N-terminal methionine.

The complex with inhibitor 1 was prepared by combining His_5-p38α at 1 mg ml^{-1} (25 μM) in buffer *C* with 125 μM inhibitor 1 from a 50 m*M* stock in DMSO to yield a final DMSO concentration of 0.25%(*v*/*v*). The inhibitor 1–p38 complex was incubated on ice for 40 min followed by 296 K for 2 h and then concentrated 5.5-fold with an Amicon Ultra 10 kDa cutoff ultrafiltration concentrator (Millipore). An equimolar amount of inhibitor 1 in 50 m*M* DMSO was spiked into the concentrated complex, incubated for 10 min at 296 K and the solution was clarified by sedimentation at 12 000*g* for 5 min to yield a final composition of 5.5 mg ml^{-1} (130 μM) His_5-p38α protein, 260 μM inhibitor 1 and 0.3%(*v*/*v*) DMSO in buffer *C*.

2.2. Preparation of inhibitor 2 complex for X-ray crystallography

The p38 protein used in the cocrystallization with inhibitor 2 was expressed by transforming N-His5-p38α-pET28a into the W3110 (DE3) strain of *E. coli* and culturing in a 1 l oxygen-sparged fermenter with enriched M101 medium [46 m*M* potassium phosphate, 23 m*M* ammonium sulfate, 4%(*w*/*v*) yeast extract (Becton Dickenson), 5%(*w*/*v*) Hy-Soy peptone (Quest Scientific), 2 m*M* magnesium sulfate, 2%(*v*/*v*) glycerol and 50 µg ml^{-1} kanamycin sulfate]. The cells were grown at 310 K to late log phase ($OD_{600\,nm}$ of 11), chilled to 293 K and induced with 1 m*M* IPTG for 16 h at 293 K before harvesting (by centrifugation) and freezing the cell paste. The His_5-p38α protein was purified at 277 K by homogenization of the cell paste at 55–62 MPa (APV Rannie Mini-Lab 8.30H) in buffer *D* [25 m*M* HEPES, 500 m*M* NaCl, 50 m*M* imidazole, 5%(*v*/*v*) glycerol, 2 m*M* 2-mercaptoethanol, 1 µg ml^{-1} leupeptin and 1 µg ml^{-1} pepstatin pH 7.5]. The lysate was clarified by ultracentrifugation (45 min at 30 000 rev min^{-1} in a Beckman Ti45 rotor) and filtration (1.2 µm syringe filter). The clarified lysate was loaded onto an Ni-affinity column (Pharmacia Biotech, Chelating Sepharose Fast Flow) equilibrated with buffer *D* and the column was eluted with a 50–500 m*M* imidazole gradient in buffer *D*. Pooled fractions were dialyzed into buffer *E* [25 m*M* HEPES, 50 m*M* NaCl, 5%(*v*/*v*) glycerol, 1 m*M* EDTA, 2 m*M* DTT and 1 µg ml^{-1} leupeptin pH 7.5] and loaded onto a 6 ml Resource Q (GE Healthcare) anion-exchange column followed by elution with an NaCl gradient to 0.6 *M* in buffer *E*. Fractions enriched in p38 protein were combined and dialyzed into buffer *F* [25 m*M* HEPES, 200 m*M* NaCl, 5%(*v*/*v*) glycerol, 1 m*M* EDTA, 2 m*M* DTT pH 7.5] and loaded onto a Pharmacia Superdex 200 (26/60) column equilibrated and eluted with buffer *F*. The final fractions were combined and dialyzed into buffer *G* [25 m*M* Tris, 50 m*M* NaCl, 5%(*v*/*v*) glycerol, 1 m*M* DTT pH 7.4]. The final purity was greater than 95% by SDS–PAGE analysis and the recovery was 350 mg purified His_5-p38α per litre of culture. The observed mass of the final product was 41 922 by electrospray ionization mass spectrometry, consistent with the predicted mass of expressed protein after the expected co-translational removal of the N-terminal methionine.

The complex of His_5-p38α with inhibitor 2 was prepared by concentrating the protein from 2.5 mg ml^{-1} in buffer *G* to 14.5 mg ml^{-1} (346 μM) with an Amicon Ultra 10 kDa molecular-weight cutoff ultrafiltration concentrator (Millipore). Inhibitor 2 from a 100 m*M* stock in DMSO was added to the 346 μM His_5-p38α solution to yield a ligand concentration of 1.72 m*M* (a fivefold molar excess) and a DMSO concentration of 1.7%(*v*/*v*) in buffer *G*. The complex was incubated at 277 K for 4 h and the solution was clarified by sedimentation at 12 000*g* for 5 min prior to crystallization.

2.3. Crystallization of p38 MAP kinase

Cocrystals of His_5-p38α with inhibitors were grown at 277 K by the hanging-drop vapor-diffusion method using VDX trays (Hampton Research). A total drop volume of 2 µl was prepared on glass cover slips (1 µl of inhibitor–p38 complex mixed with 1 µl reservoir solution) inverted over 1 ml reservoir solution containing 1–6%(*w*/*v*) PEG 4K in 50 m*M* MES pH 6.0, 5 m*M* magnesium sulfate. Crystals appeared spontaneously within one week, but could be observed in 1–2 d as more single perfect crystals when the drops were microseeded by streaking with a cat whisker dipped in a diluted suspension of crushed inhibitor 1 cocrystals in 5%(*w*/*v*) PEG 4K, 50 m*M* MES pH 6.0, 5 m*M* magnesium sulfate. To prevent the crystals from cracking during cryopreservation, a slow serial transfer of 5 × 0.25 µl cryosolution (25% glycerol in mother liquor) was added to the 2 µl drops *in situ* over 2 h at 277 K prior to harvesting with a cryoloop, quickly dipping into a fresh drop of cryosolution and plunging into liquid nitrogen.

2.4. Data collection and reduction

Data were collected on the IMCA-CAT beamlines at the Advanced Photon Source, Argonne, Illinois, USA. Data for p38 MAP kinase complexed with inhibitor 1 were collected to 1.7 Å resolution with an ADSC area detector on beamline ID-17 and data for p38 MAP kinase complexed with inhibitor

Table 2
Data-collection statistics.

Values in parentheses are for the highest resolution bin.

	Inhibitor 1	Inhibitor 2
	PDB code 2rg6	PDB code 3bv3
Date of data collection	10 November 2006	29 September 2001
Temperature (K)	100	100
X-ray source	APS ID-17	APS BM-17
Detector	ADSC Q210	MAR CCD
Crystallographic space group	$P2_12_12_1$	$P2_12_12_1$
Real-space cell *a* (Å)	69.1	66.3
Real-space cell *b* (Å)	71.4	74.9
Real-space cell *c* (Å)	80.5	78.8
Data-reduction program	*HKL*-2000	*HKL*-2000
Resolution range (Å)	53.5–1.72 (1.78–1.72)	50.0–2.59 (2.73–2.59)
No. of reflections collected	311289 (25842)	66989 (4166)
No. of unique reflections	43003 (4205)	12467 (1175)
Data redundancy	7.2 (6.8)	4.4 (3.8)
Completeness (%)	99.8 (99.0)	97.8 (97.2)
$R_{\rm merge}$† (%)	7.0 (32.4)	10.8 (69.4)
Average $I/\sigma(I)$	25.3 (5.1)	17.3 (2.3)

† $R_{\rm merge} = \sum_{hkl}\sum_i |I_i(hkl) - \langle I(hkl)\rangle|/\sum_{hkl}\sum_i I_i(hkl)$, where $\langle I(hkl)\rangle$ is the mean intensity of the i reflections with intensity $I_i(hkl)$ and common indices *hkl*.

Table 3
Refinement parameters.

Values in parentheses are for the highest resolution bin.

	Inhibitor 1	Inhibitor 2
	PDB code 2rg6	PDB code 3bv3
Refinement program	*AutoBUSTER*	*AutoBUSTER*
Resolution range (Å)	53.5–1.72 (1.82–1.72)	50.0–2.59 (2.75–2.59)
Completeness (%)	99.6 (99.6)	97.8 (97.8)
No. of reflections used	42947 (6761)	12461 (1884)
R value† (%)	20.0 (21.0)	19.8(24.5)
Free *R* value‡ (%)	22.1 (24.4)	28.4 (28.8)
Estimated *B* value (Wilson) (Å^2)	23.2	62.5
Mean *B* value (Å^2)	24.2	54.4
Mean *B* factor (ligand) (Å^2)	22.7	41.35
R.m.s. deviations		
Bond lengths (Å)	0.008	0.006
Bond angles (°)	1.1	0.9
Torsion angles (°)	16.9	27.5
Residues in final model	335	338
Total No. of atoms	3069	2869
Protein atoms	2704	2731
Ligand atoms	68	44
Solvent atoms	297	94

† R value $= \sum_{hkl}\big||F_{\rm obs}| - |F_{\rm calc}|\big|/\sum_{hkl}|F_{\rm obs}|$, where $F_{\rm obs}$ and $F_{\rm calc}$ are the observed and calculated structure factors, respectively. ‡ For the free R value, the sum is extended over a subset of reflections (~5%) excluded from all stages of refinement.

2 were collected to 2.3 Å resolution with a MAR area detector on beamline BM-17. The data were reduced with the programs *DENZO* and *SCALEPACK* (Otwinowski & Minor, 1997). Crystallographic data-collection and reduction statistics are summarized in Table 2.

2.5. Structure determination and refinement

The initial structures were determined by the molecular-replacement method with *AMoRE* (Navaza, 1994) using the refined model of p38 map kinase (PDB code 1wfc; Wilson *et al.*, 1996) as the search model.

The structures were refined with the program *autoBUSTER* (Global Phasing Ltd, Cambridge, England) and were examined and manually refitted with the program *CHAIN* (v.9.0; Sack & Quiocho, 1997). The difference electron density clearly defined the position of the inhibitor in the ATP-binding pocket. Additional cycles of refinement were performed to add solvent molecules. The final crystallographic refinement statistics are summarized in Table 3.

3. Results and discussion

3.1. Overall structures

The crystal structure of p38 MAP kinase in the presence of the pyrrolotriazine inhibitor 1 has been determined at 1.72 Å resolution to an *R* factor of 20.0% ($R_{\rm free}$ = 22.1%); the crystal structure with inhibitor 2 has been determined at 2.59 Å resolution to an *R* factor of 19.8% ($R_{\rm free}$ = 28.4%). With the exception of the activation loop and the immediate vicinity of the binding site, the overall structure of p38 MAP kinase with the inhibitors bound is virtually identical to that of the apo unphosphorylated protein, as previous reported (Wilson *et al.*, 1996; Wang *et al.*, 1997). In the structures reported here, loop 31–34 (between β-strands 1 and 2) and the activation loop 171–183 are not well defined in the electron-density maps and have been excluded from the model.

3.2. Binding mode of pyrrolotriazine inhibitor 1

As expected, the pyrrolotriazine inhibitor 1 binds in the ATP-binding site (Fig. 2*a*). The pyrrolotriazine ring sits in the adenine pocket, but does not make any hydrogen-bond interactions with the protein (the closest distance is 3.5 Å). This is in contrast to the related quinazolinone-based inhibitors, in which the core group interacts with Met109 (Cumming *et al.*, 2004). In inhibitor 1, it is the adjacent amide that makes the ubiquitous interaction with the main-chain amino group of Met109. The chiral α-methylbenzyl group sits at the edge of the binding site as observed previously in a pyridinyl-imidazole inhibitor (Fitzgerald *et al.*, 2003).

On the other side of the pyrrolotriazine, the *ortho*-methyl group points towards the carboxyl of Ala51 and the side chain of Thr106. It has been proposed that interactions in this hydrophobic pocket may partially be responsible for the specificity of inhibitors of p38 (Cherry & Williams, 2004). The diarylamide linker makes hydrogen-bond interactions between the nitrogen and the side chain of Glu71 and, on the opposite side, between the carboxyl and the main-chain amino of Asp168.

The methoxyamide points towards the interior, with the nitrogen and oxygen pointing towards Glu71 and Leu75 of the hydrophobic pocket and the methyl group pointing directly at the DFG portion of the activation loop. However, the methoxyamide does not make a hydrogen-bond interaction (the closest approach is 3.25 Å). The remaining portion of the activation loop is not observed in the structure owing to significant disorder. Neither the regions that normally interact with the ATP ribose (Asp112 and Ser154) or terminal phosphate (near Tyr35) are utilized by the inhibitor.

3.3. Binding mode of pyrrolotriazine nhibitor 2

Inhibitor 2, which differs from inhibitor 1 by the replacement of methoxyamide with the benzylmorpholine group, binds in a nearly identical mode, except for a slight rotation of the toluene group in the inhibitor. The same interactions with the hinge region and with the main chain of Asp168 are observed (Fig. 2*b*). However, the replacement of the methoxyamide by a benzylmorpholine group extends the ligand approximately 6 Å deeper into the pocket occupied by the DFG loop. This would cause the morpholino group to clash with the position of Phe169 as found in the inhibitor 1 structure. In order to accommodate this large group, the DFG loop must adopt an 'out' conformation. The phenylalanine flips out of position and now points towards the exterior of the protein near residues Glu71 and Arg67 (Fig. 3).

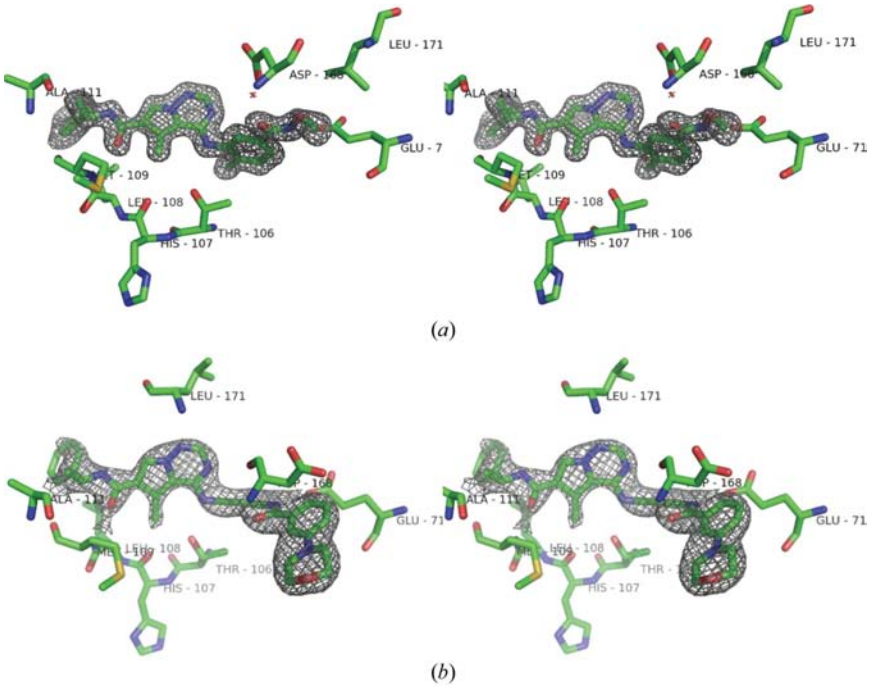

Figure 2
Electron-density map of (*a*) inhibitor 1 and (*b*) inhibitor 2 bound to p38 MAP kinase. Figs. 2, 3 and 4 were drawn using *PyMOL* (DeLano Scientific LLC, San Carlos, USA).

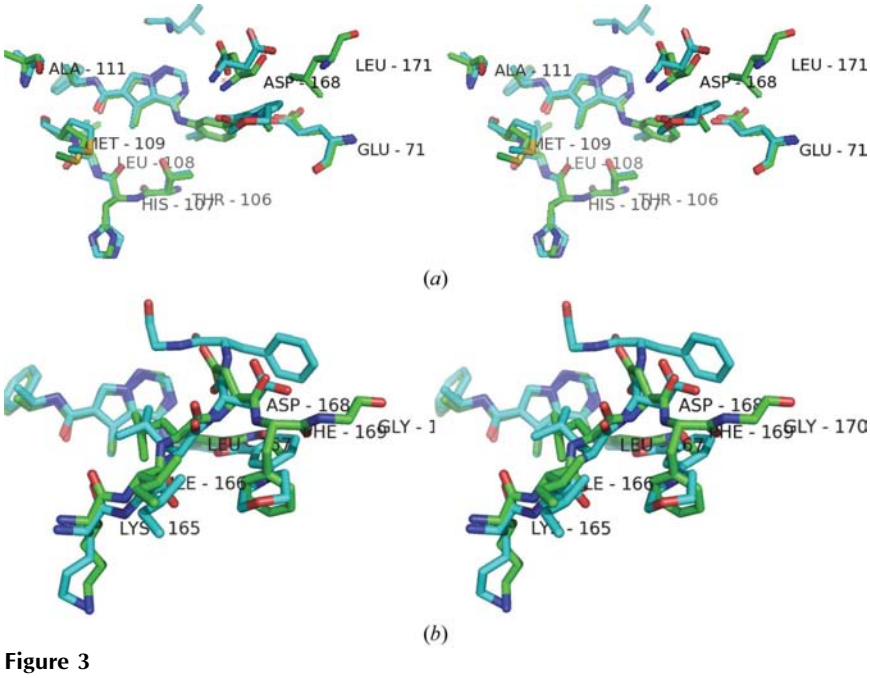

Figure 3
(*a*) Overlap of inhibitor 1 (green) and inhibitor 2 (cyan) in the binding site. (*b*) Comparison of DFG movement in inhibitor 1 (green) and inhibitor 2 (cyan).

The morpholine sits in the hydrophobic pocket opened up by the movement of Phe169 formed by Leu74, Ile141, Ile146 and His148. The morpholino O atom is close to two C atoms: Ile141 $C^{\delta1}$ (3.3 Å) and His148 $C^{\delta2}$ (3.5 Å).

As a consequence of the flip of the DFG loop, several additional interactions can occur. A water molecule is now observed in the binding site, forming an interaction between the 3-nitrogen position of the pyrrolotriazine, the side-chain N atom of Lys53 and the carboxyl of Asp168. Two residues (Leu171 and Ala172) can now be visualized in the activation loop of the inhibitor 2 structure which lacked electron density in the inhibitor 1 structure. This may be the result of the stabilization of these residues owing to a new interaction between the main-chain carboxyl of Leu171 and the amino of the α-methylbenzyl amide.

The design of another high-affinity (Table 1) morpholine-containing p38 inhibitor, BIRB-796 (Fig. 4*a*), which also interacts both with Met109 of the hinge region and forces the protein to adopt the DFG-out conformation has been described previously (Regan *et al.*, 2002; PDB code 1kv2). In that structure, the protein adopts a very different conformation compared with that observed in the inhibitor 2 structure and Phe169 sits in a different position between Ser154 and the ethoxy linker of the inhibitor. The morpholino group is oriented in the opposite direction and accepts a hydrogen bond from Met109. The carboxyl is in position to accept a hydrogen bond from the main-chain amino group of Asp168. With BIRB-796, it is the *t*-butyl group on the opposite end of the ligand (near the position of the morpholine in inhibitor 2) that is in the location normally occupied by Phe169. The methylbenzene is pointed towards Arg70 and Glu71; this is near the position into which Phe169 has flipped in structure 2. The phenylalanine in the BIRB-796 complex is in a position occupied by the main chain of

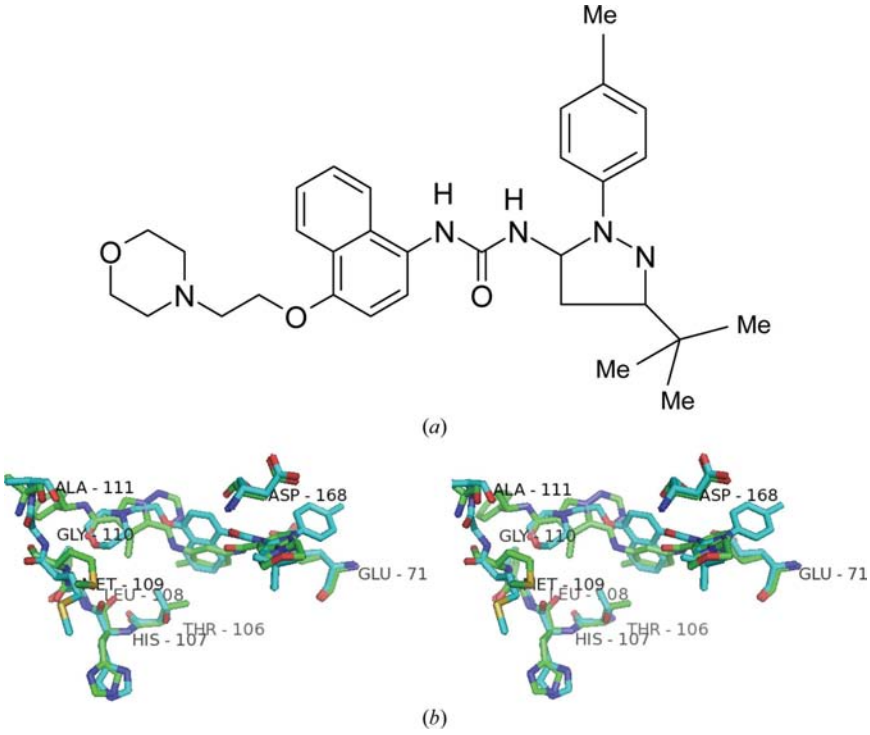

Figure 4
(*a*) Structure of BIRB-796. (*b*) Comparison of DFG movement in the inhibitor 2 (green) and BIRB-796 (cyan) complexes.

Gly170 in the inhibitor 2 complex (Fig. 4*b*). The remainder of the activation loop is not visible in either structure and is presumably disordered.

4. Conclusions

The crystallographic structures of p38 MAP kinase with two pyrrolotriazine-based inhibitors reveal the binding mode of this series of inhibitors as well as demonstrating the flexible nature of the ATP-binding site. The smaller inhibitor 1, with a methoxyamide group, can be accommodated without movement of the activation loop. Replacement of the methyoxyamide by a benzylmorpholino group extends the ligand into the region in which the DFG region of the activation loop normally resides, forcing movement of the DFG loop, and allows the ligand to make a new series of interactions with residues Ile141 and His148. These additional interactions may play a role in the higher affinity, IC_{50} = 0.4 *versus* 2.2 n*M*, of inhibitor 2 compared with inhibitor 1.

Designing extended inhibitors that purposely force the DFG loop to flip out of position and make interactions with the new hydrophobic pocket may be a way to increase their binding affinity. It may also suggest a mechanism to add specificity to p38 inhibitors, particularly against other kinases which have activation loops that are more rigidly fixed and cannot easily adapt the DFG-out conformation needed to accommodate such extended ligands.

We thank Shuqun Lin and Dr Steven Wrobleski for providing the compounds used in this study, Li Tao and Bethanne Warrack for mass-spectrometric analysis and Dr Eric Baldwin, Dr Arthur Doweyko, Dr Herbert Klei, Dr Steven Sheriff and Dr Katerina Leftheris for helpful discussions and assistance in the preparation of this manuscript. We also thank the staff of the IMCA-CAT beamline 17-ID at the Advanced Photon Source, Argonne, Illinois, USA. The use of the beamline was supported by the companies of the Industrial Macromolecular Crystallography Association through a contract with the Center for Advanced Radiation Sources at the University of Chicago.

References

Adams, J. L., Badger, A. M., Kumar, S. & Lee, J. C. (2001). *Prog. Med. Chem.* **38**, 1–60.
Cherry, M. & Williams, D. H. (2004). *Curr. Med. Chem.* **11**, 663–673.
Cumming, J. G., McKenzie, C. L., Bowden, S. G., Campbell, D., Masters, D. J., Breed, J. & Jewsbury, P. J. (2004). *Bioorg. Med. Chem. Lett.* **14**, 5389–5394.
Fitzgerald, C. E., Patel, S. B., Becker, J. W., Cameron, P. M., Zaller, D., Pikounis, V. B., O'Keefe, S. J. & Scapin, G. (2003). *Nature Struct. Biol.* **10**, 764–769.
Hynes, J. Jr *et al.* (2008). *J. Med. Chem.* **51**, 4–16.
Kumar, S., Boehm, J. & Lee, J. C. (2003). *Nature Rev. Drug. Discov.* **2**, 717–726.
Lisnock, J., Tebben, A., Frantz, B., O'Neill, E. A., Croft, G., O'Keefe, S. J., Li, B., Hacker, C., de Laszlo, S., Smith, A., Libby, B., Liverton, N., Hermes, J. & LoGrasso, P. (1998). *Biochemistry*, **37**, 16573–16581.
Navaza, J. (1994). *Acta Cryst.* A**50**, 157–163.
Otwinowski, Z. & Minor, W. (1997). *Methods Enzymol.* **276**, 307–326.
Pargellis, C., Tong, L., Churchill, L., Cirillo, P. F., Gilmore, T., Graham, A. G., Grob, P. M., Hickey, E. R., Moss, N., Pav, S. & Regan, J. (2002). *Nature Struct. Biol.* **9**, 268–272.
Regan, J. *et al.* (2002). *J. Med. Chem.* **45**, 2994–3008.
Sack, J. S. & Quiocho, F. A. (1997). *Methods Enzymol.* **277**, 158–173.
Saklatvala, J. (2004). *Curr. Opin. Pharmacol.* **4**, 372–377.
Stelmach, J. E. *et al.* (2003). *Bioorg. Med. Chem. Lett.* **13**, 277–280.
Tong, L., Pav, S., White, D. M., Rogers, S., Crane, K. M., Cywin, C. L., Brown, M. L. & Pargellis, C. A. (1997). *Nature Struct. Biol.* **4**, 311–316.
Trejo, A. *et al.* (2003). *J. Med. Chem.* **46**, 4702–4713.
Wang, Z., Harkins, P. C., Ulevitch, R. J., Han, J., Cobb, M. H. & Goldsmith, E. J. (1997). *Proc. Natl Acad. Sci. USA*, **94**, 2327–2332.
Wilson, K. P., Fitzgibbon, M. J., Caron, P. R., Griffith, J. P., Chen, W., McCaffrey, P. G., Chambers, S. P. & Su, M. S.-S. (1996). *J. Biol. Chem.* **271**, 27696–27700.
Wrobleski, S. T. *et al.* (2008). *Bioorg. Med. Chem. Lett.* **18**, 2739–2744.